Journal of Molecular Catalysis A: Chemical 335 (2011) 145–150

Contents lists available at ScienceDirect

Journal of Molecular Catalysis A: Chemical

journal homepage: www.elsevier.com/locate/molcata

Enhanced sunlight photocatalytic performance of Sn-doped ZnO for Methylene Blue degradation

Jian-Hui Sun, Shu-Ying Dong, Jing-Lan Feng*, Xiao-Jing Yin, Xiao-Chuan Zhao

Henan Key Laboratory for Environmental Pollution Control, College of Chemistry and Environmental Sciences, Henan Normal University, Jianshe Road, Xinxiang, Henan 453007, PR China

ARTICLE INFO

Article history:
Received 2 September 2010
Received in revised form
23 November 2010
Accepted 24 November 2010
Available online 2 December 2010

Keywords:
ZnO
Sn-doped ZnO
Photocatalytic
Sunlight
Methylene Blue

ABSTRACT

In the present study, nano-structured ZnO and Sn-doped ZnO photocatalysts with high sunlight photocatalytic activity were successfully synthesized through the decomposition of zinc acetate and glucose by microwave heating. The prepared ZnO and Sn-doped ZnO photocatalyst were characterized by X-ray diffraction (XRD), scanning electron microscopy (SEM), photoluminescence spectrum (PL), UV–vis absorption spectrum (UV–vis), N_2 adsorption and UV–vis diffuse reflectance spectra (DRS). The results showed that the doping greatly changed the microstructure, morphology and optical properties of ZnO, which may contribute to the enhancement of photocatalytic activity. The sunlight photocatalytic activity of the prepared pure ZnO and Sn-doped ZnO photocatalyst was investigated by the degradation of Methylene Blue (MB) solution under sunlight irradiation. Compared with pure ZnO, 13% higher decolorization rate and 29–52% higher mineralization efficiency were obtained by the Sn-doped ZnO. The results indicated that Sn-doped ZnO had a higher photocatalytic activity and Sn dopant greatly increased the photocatalytic activity of ZnO.

1. Introduction

Environmental pollutions caused by pesticides, dyes and heavy metal in water have provided the motivation to sustained fundamental and applied research interest in the area of environmental remediation [1,2]. Heterogeneous photocatalytic degradation of refractory organic pollutants from water by semiconductors has attracted extensive attention in the past several decades [3–5]. Previous studies have proved that the wide-bandgap semiconductor photocatalyst such as TiO_2 and ZnO can degrade various organic pollutants under UV irradiation, which offers great potentials for the complete elimination of toxic chemicals [6,7]. It has been reported that ZnO had higher photocatalytic efficiency compared with TiO_2 in the degradation of several organic contaminants in both acidic and basic medium, which has stimulated many researchers to further explore the properties of ZnO in many photocatalytic reactions [8–10]. The biggest advantage of ZnO compared with TiO_2 is that it absorbs over a larger fraction of the UV spectrum and absorbs more light quanta than TiO_2 [11,12].

However, the photocatalyst needs to be further improved before its commercialization due to the fast recombination rate of the photogenerated electron/hole pairs in this technology [13]. Therefore, suppression of the recombination of photogenerated electron–hole pairs in the semiconductors is essential for improving the efficiency of photocatalytic [14]. Doping is a very useful way to improve the charge separation in semiconductor systems, many dopants such as Sb, Er and Al have been used [15,16]. Especially, Sn was considered as one of the most important doping elements for ameliorating the photocatalytic activity of ZnO [17].

It has been demonstrated that the structural and morphological characters such as the size, shape, crystalline form, photocatalytic activity and some relevant properties of ZnO can be significantly affected by different synthesis methods [18]. Various methods have been developed to prepare ZnO photocatalyst with special performance, which mainly include template method, precipitation, gas-phase reaction, hydrothermal synthesis and microwave heating [19–22]. In recent years, it has been reported that glucose could be used as co-catalyst, reductant and assistant to prepare various materials [23–25]. For example, Yu and Yu [25] successfully synthesized hollow ZnO spheres using $ZnCl_2$ and glucose as starting materials, which confirmed that glucose could prevent the crystallization of ZnO due to the metal precursors disperse in the hydrophilic shell of the carbon spheres as amorphous clusters before calcinations. However, synthesis of ZnO or Sn-doped ZnO photocatalyst through the decomposition of zinc acetate and glucose by microwave heating has not been reported.

The aim of this study is to synthesize ZnO and Sn-doped ZnO photocatalyst through the decomposition of zinc acetate and glu-

* Corresponding author. Tel.: +86 373 3325971; fax: +86 373 3326336.
E-mail addresses: fengjl1123@yahoo.com.cn, fengjinglan@gmail.com (J.-L. Feng).

1381-1169/$ – see front matter © 2010 Elsevier B.V. All rights reserved.
doi:10.1016/j.molcata.2010.11.026

cose by microwave heating. The microstructure, morphology and optical properties changes of the prepared photocatalyst by doping were systematically characterized by X-ray diffraction (XRD), scanning electron microscopy (SEM), photoluminescence spectrum (PL), UV–vis absorption spectrum (UV–vis), N_2 adsorption and UV–vis diffuse reflectance spectra (DRS). The sunlight photocatalytic activity of the prepared photocatalyst was evaluated by the degradation of Methylene Blue (MB) under sunlight irradiation.

2. Materials and methods

2.1. Materials

Zinc acetate dihydrate ($Zn(CH_3COO)_2{\cdot}2H_2O$) and glucose ($C_6H_{12}O_6$) were purchased from Tianjin Chemical Reagents Factory (Tianjin, China). Methylene Blue and $SnCl_2{\cdot}2H_2O$ were purchased from Shanghai Chemical Reagent Company (Shanghai, China).

Reagents for COD analysis include ferrous ammonium sulphate ($(NH_4)_2Fe(SO_4)_2{\cdot}6H_2O$), potassium dichromate ($K_2Cr_2O_7$), silver sulphate (Ag_2SO_4), mercury sulphate ($HgSO_4$), 1,10-Phenanthroline ($C_{12}H_8N_2{\cdot}H_2O$), ferrous sulphate ($FeSO_4{\cdot}7H_2O$) and sulphuric acid (H_2SO_4). All the chemicals were analytical grade reagents and used without further purification. Deionized water with conductivity between 0.7 and 1.0 $\mu S\,cm^{-1}$ was used throughout this study.

2.2. Preparation of ZnO and Sn-doped ZnO photocatalyst

All the samples were prepared by microwave heating and $Zn(CH_3COO)_2{\cdot}2H_2O$, $C_6H_{12}O_6$ and $SnCl_2{\cdot}2H_2O$ were used as the main materials. In a typical procedure, 5 g $Zn(CH_3COO)_2{\cdot}2H_2O$ and 15 g $C_6H_{12}O_6$ were dissolved in 15 mL deionized water, then added 0.8 mL H_2SO_4 (98%), the reaction mixture was poured into a PTFE sealed can and heated in a microwave oven (Midea KD21B-C, 2.45 GHz, Shunde Medea Microwave Oven Production Co. Ltd., Foshan, China) at a power of 800 W for 1 min, followed by cooled for 20 min, cycle this procedure for 4 times. After that the PTFE sealed can was cooled down to room temperature, the brown colloid material was filtered and washed with deionized water in order to remove undesirable anions such as CH_3COO^-, Cl^- and SO_4^{2-}, dried at 80 °C for 5 h and then calcined at 700 °C for 2 h. Sn doping solution was prepared exactly like the pure one by dissolving 0.1 g $SnCl_2{\cdot}2H_2O$ into the reaction mixture.

2.3. Characterizations

The crystal structure of the prepared ZnO and Sn-doped ZnO photocatalyst was analyzed by XRD. The patterns were recorded in the 2θ range of 20–80° with a scan rate of 0.02°/0.4 s by using a Bruker-D8-AXS diffractometer system equipped with a Cu Kα radiation (λ = 0.15406 Å) (Bruker Co., Germany). The morphology and dimensions of photocatalysts were observed by SEM (JSM-6301, Japan). The PL spectra of photocatalysts were measured using a Fluorescence Spectrophotometer (FP-6500, Japan) equipped with a Xenon lamp at an excitation wavelength of 325 nm. The UV–vis spectra of photocatalysts were measured by using a UV–vis spectrophotometer (Lambda 17, Perkin-Elmer), prior to UV–vis analysis the ZnO samples was ultrasonically dispersed in deionized water at room temperature. The low temperature N_2 adsorption was procedured using a Micromeritics ASAP 2020 apparatus at −196 °C, all the samples were degassed at 100 °C for 6 h before the measurement. The specific surface area was calculated by BET method. The pore diameter distribution was calculated using the BJH model based on the desorption isotherm. UV–vis diffuse reflectance spectra (DRS) were obtained using a Shimadzu UV-3600 spectrometer by using $BaSO_4$ as a reference, with the spectra were measured in the range 200–800 nm.

2.4. Sunlight photocatalytic activity test

Photocatalytic experiments were carried out in a 500 mL capacity borosilicate photochemical batch reactor having dimensions 15 cm × 10 cm (height × diameter). All photocatalytic experiments were performed under similar conditions on sunny days between 8:30 A.M. and 6:30 P.M. (the reaction time was 10 h), April–May. The ambient temperature was between 26 °C and 33 °C. The dye solutions were prepared using deionized water. 300 mL 40 mg L^{-1} MB solution was added to the reactor and then covered with thin glass plate in order to decrease the evaporation of solution under sunlight irradiation. The dye wastewater was in its natural pH (about 6.7) and no pH control was conducted during the whole photocatalytic degradation experiments. In all experiments, 0.1 g photocatalyst was added to the dye aqueous solutions and magnetically stirred (300 rpm) in dark for 30 min, in order to achieve adsorption–desorption equilibrium between dye and catalyst. After that, the suspension was irradiated with sunlight and photocatalytic experiment was started. Samples were periodically taken out for analysis.

2.5. Analytical methods

The photocatalytic degradation of MB was monitored by withdrawing 3 mL samples at regular intervals and immediately centrifuged (2000 rpm) to remove particles for analysis. The decolorization efficiency of MB was tested in terms of the changes of the UV–vis absorbance of MB. The absorbance intensity of MB was determined by an UV–vis spectrophotometer (Lambda 17, Perkin-Elmer) with a 1 cm path length spectrometric quartz cell.

The mineralization of MB was measured by the decrease of chemical oxygen demand (COD) and total organic carbon (TOC) of the dye solution. COD was measured according to the standard dichromate titration method [26]. TOC was measured by a TOC analyzer (Apollo 9000, Terkmar–Dohrmann, USA). The mineralization efficiency of MB was estimated by the following expression,

$$\text{Mineralization of MB}\,(\%) = \left(1 - \frac{\text{COD}_t \text{ or } \text{TOC}_t}{\text{COD}_0 \text{ or } \text{TOC}_0}\right) \times 100 \qquad (1)$$

where COD_0 and TOC_0 is the COD and TOC concentration after 30 min adsorption–desorption equilibrium, COD_t and TOC_t is the COD and TOC concentration at certain reaction time t (h), respectively.

3. Results and discussion

3.1. Characterizations of the ZnO and Sn-doped ZnO photocatalyst

The XRD spectra of the prepared ZnO and Sn-doped ZnO photocatalyst are shown in Fig. 1. A series of characteristic peaks: 2.8143 (1 0 0), 2.6033 (0 0 2), 2.4759 (1 0 1), 1.9111 (1 0 2), 1.6247 (1 1 0), 1.4771 (1 0 3), 1.4072 (2 0 0), 1.3782 (1 1 2), 1.3583 (2 0 1), 1.3017 (0 0 4) and 1.2380 (2 0 2) are observed in Fig. 1a and b, which are in accordance with those of the hexagonal wurtzite structure of ZnO (International Center for Diffraction Data, JCPDS 36-1541). The diffraction peaks of the pure ZnO (Fig. 1a) are sharp and intense, revealing the highly crystalline character of the ZnO sample, while the diffraction peaks of the Sn-doped ZnO are broad and weak (Fig. 1b), indicating a small crystal size or semicrystalline nature of this sample [27]. All diffraction peaks in Fig. 1b are correspondingly ascribed to Zinc Tin Oxide ($ZnSnO_3$). Furthermore, it is worthwhile

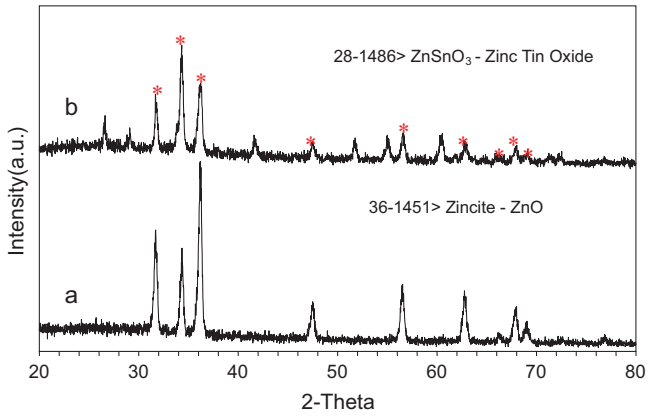

Fig. 1. XRD patterns of the as-synthesized samples: (a) pure ZnO, (b) Sn-doped ZnO.

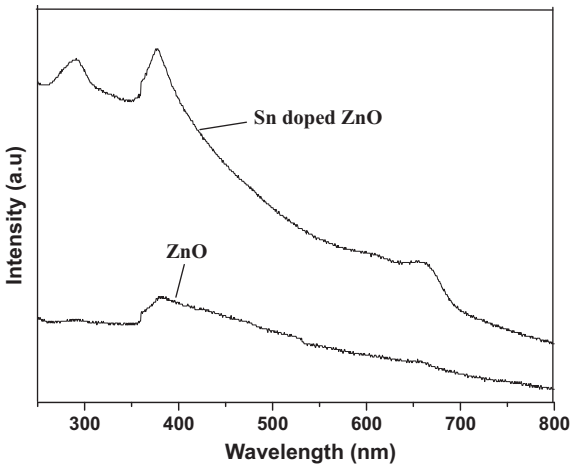

Fig. 3. The UV–vis absorption spectra of the pure ZnO and Sn-doped ZnO photocatalyst.

to note that the diffraction peaks of ZnO nanocrystals in the Sn-doped ZnO sample are still very sharp despite the weak intensity, implying the highly crystalline character of ZnO nanocrystals in this sample.

SEM images of the synthesized pure ZnO (Fig. 2a and b) and Sn-doped ZnO (Fig. 2c and d) photocatalyst are shown in Fig. 2. From Fig. 2a and b, it can be seen that nano-sized ZnO photocatalyst was successfully synthesized, the shape of the prepared pure ZnO photocatalyst looks like rice and with average particle size of about 100 nm in diameter and 300 nm in length. After doping Sn, the morphologies of Sn-doped ZnO photocatalyst as shown in Fig. 2c and d are significantly different from the pure ZnO. The shape of the prepared Sn-doped ZnO looks like diamond and with average particle size of about 300 nm. Although the pure ZnO show a smaller particle size than the Sn-doped ZnO photocatalyst, it also can be seen from Fig. 2 that the pure ZnO particles are more easily to agglomerate with each other, which could result in the decreasing light utilization rate. Though the agglomeration problem of pure ZnO can be solved by doping Sn, the microstructures of Sn-doped ZnO photocatalyst become a little uneven.

Fig. 3 shows the comparison of UV–vis absorption spectra of the prepared pure ZnO and Sn-doped ZnO photocatalyst at room temperature. It can be seen that the doping has greatly changed the light absorption of the photocatalyst. An absorption peak centered at 375 nm is found in two spectra, but there are other two peaks centered at 290 nm and 650 nm in the Sn-doped ZnO. As shown in Fig. 3, the prepared pure ZnO and Sn-doped ZnO photocatalyst had a broad absorption band from ultraviolet to visible region and the absorbance of the photocatalyst slightly decreases as the wavelength increases, which indicate that the prepared ZnO photocatalyst has a potential capacity of photocatalytic activity utilizing sunlight. It is well known that the optical absorption behavior of photocatalyst significantly affects the photocatalytic activity of

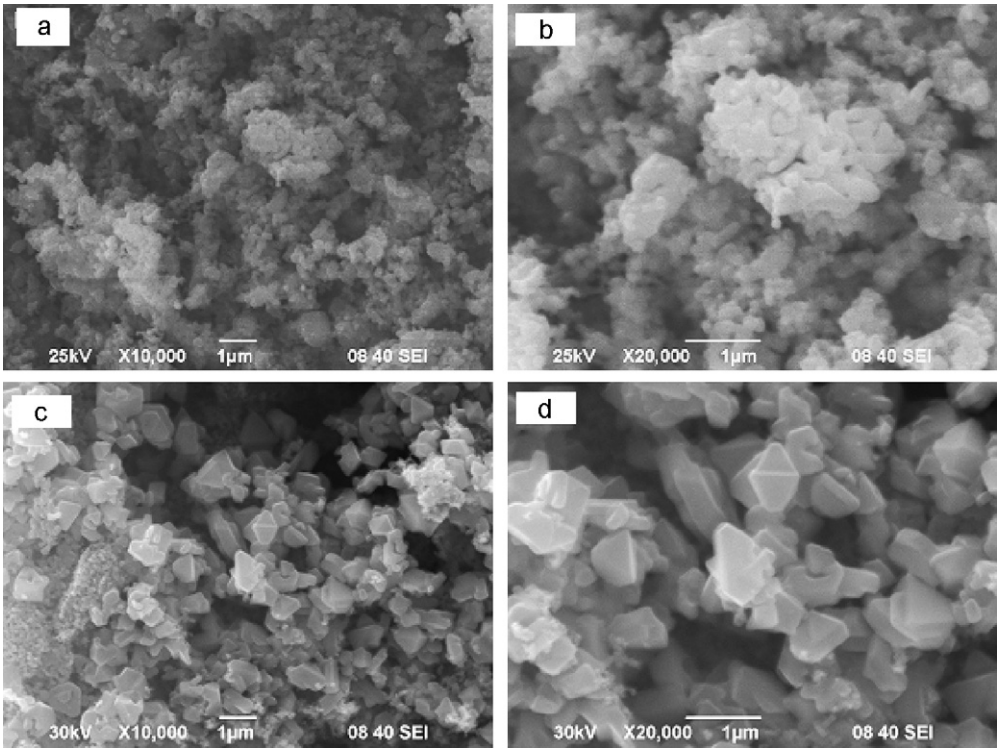

Fig. 2. SEM images of the synthesized pure ZnO (a and b) and Sn-doped ZnO (c and d) photocatalyst.

Table 1
Nitrogen adsorption characteristics of the pure ZnO and Sn-doped ZnO.

Sample	BET surface area[a] (m^2/g)	Pore volume[b] (cm^3/g)	Pore diameter[c] (nm)
Pure ZnO	4.0	0.02	30–50, 35
Sn-doped ZnO	3.8	0.06	41–78, 50

[a] BET surface area calculated from the linear part of the BET plot (p/p^0 = 0.07–0.22).
[b] Total pore volume, taken from the volume of N_2 adsorbed at p/p^0 = 0.974.
[c] Average pore diameter, estimated using the desorption branch of the isotherm and the Barrett–Joyner–Halenda (BJH) formula.

the photocatalyst [28–30]. In general, the red-shift in the absorption band edge and the increase in absorption intensity attributed to the increased formation rate of electron–hole pairs on the photocatalyst surface, resulting in the photocatalyst exhibiting higher photocatalytic activity. The similar results were reported in Ref [31]. It is not difficult to conjecture that the Sn-doped ZnO has a higher photocatalytic activity.

The specific surface area is an important microstructural parameter of ZnO particles, which depends on the geometrical shape and porosity of the particles [32]. The results of measurements for BET surface area, pore volume and pore diameters are summarized in Table 1. The specific BET surface areas of pure ZnO and Sn-doped ZnO were found to be 4 and 3.8 m^2/g respectively, which are in accordance with the results of SEM that the pure ZnO has smaller particle size. The significant difference between pure ZnO and Sn-doped ZnO could be found both in the pore diameter and pore volume, the samples show broad distribution of pores with a average pore diameter 35 and 50 nm, respectively, and the corresponding single-point total pore volume at p/p^0 = 0.974 are 0.02 and 0.06 cm^3/g, respectively.

Fig. 4 shows PL spectra of the prepared pure ZnO and Sn-doped ZnO photocatalyst. It was found that the spectrum of the prepared pure ZnO and Sn-doped ZnO photocatalyst were similar, only one broad luminescence band covered from 430 to 550 nm, which can be assigned to blue-green regions, but the PL intensity were different. It has been reported that the blue-green emission is caused by the recombination of electrons in single occupied oxygen vacancies [33]. The PL spectra show oxygen vacancies or other point defects might be present in the prepared ZnO photocatalyst. Since PL emission was the result of the recombination of excited electrons and holes, the lower PL intensity of the prepared ZnO indicated a lower recombination rate of excited electrons and holes [34]. As shown in Fig. 4, the prepared Sn-doped ZnO had the lower recombination rate of electrons and holes than the pure ZnO, may leading to higher photocatalytic oxidation activity.

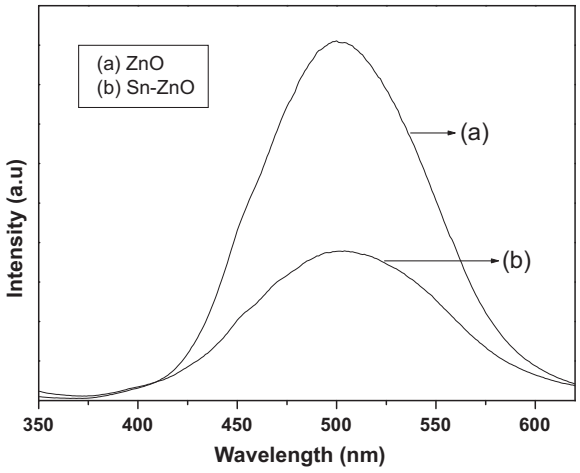

Fig. 4. The PL spectra of the prepared pure ZnO and Sn-doped ZnO photocatalyst.

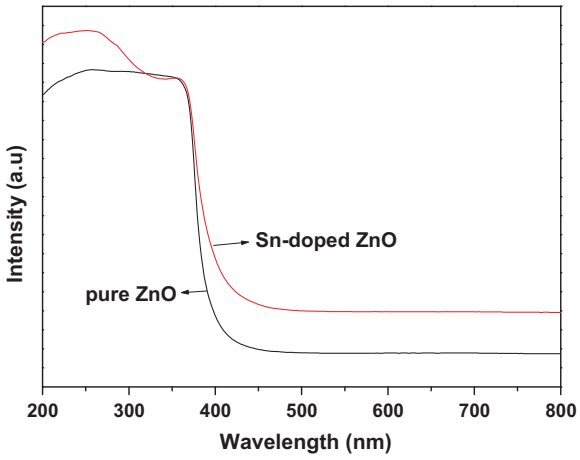

Fig. 5. UV–vis diffuse reflectance spectra (DRS) of pure ZnO and Sn-doped ZnO.

Fig. 5 shows the DRS spectra of pure ZnO and Sn-doped ZnO, which show broad intense absorption from 430 nm to lower wavelengths, are typically associated with a change-transfer process from the valence band to conduction band. The absorption band from 200 nm to 260 nm can be assigned to $O^{2-} \rightarrow Sn^{4+}$ charge transfer transition of the Sn ions in a tetrahedral and octahedral environment [35]. It is well known that the band gap of ZnO is 3.2 eV, it can be excited by photons with wavelengths below 387 nm. From Fig. 5, it can be seen that, the curve of Sn-doped ZnO has a clear absorption in the visible range, beside the absorption edge near 400 nm. It is clearly that the absorption wavelength range of Sn-doped ZnO red shifts to visible light, which can be easily excited by sunlight.

3.2. Comparison of the solar photocatalytic activity of the pure ZnO and Sn-doped ZnO photocatalyst

3.2.1. Decolorization of MB wastewater

In the absence of pure ZnO and Sn-doped ZnO photocatalyst, the sunlight photolysis of 40 mg L^{-1} MB in aqueous solution was tested. It was found that no significant changes of the concentration of MB after 10 h irradiation (data was not shown), which indicated that MB cannot be easily degraded by sunlight photolysis. Fig. 6 shows the UV–vis adsorption changes of MB in the presence of 0.1 g pure ZnO (Fig. 6a) and Sn-doped ZnO (Fig. 6b) under sunlight irradiation. Before reaction, three absorbance peaks at 243, 286 and 664 nm can be observed from the UV–vis absorbance spectrum of MB solution. The peaks at 243 and 286 nm are attributed to the absorbance of $\pi \rightarrow \pi^*$ transition, while the peak at 664 nm is attributed to the absorbance of $n \rightarrow \pi^*$ transition [36]. It can be seen from Fig. 6a and b that the MB decreased dramatically as the reaction time increased. According to changes of the absorbance intensity at 664 nm, the decolorization efficiency of 40 mg L^{-1} MB solutions in the presence of pure ZnO (Fig. 6a) and Sn-doped ZnO (Fig. 6b) after 4 h photocatalytic reaction was achieved 50% and 80%, respectively. Complete decolorization of MB in the presence of Sn-doped ZnO was achieved within 6 h, while the decolorization of MB in the presence of pure ZnO was achieved 87% even after 10 h sunlight irradiation. The results indicated that the Sn-doped ZnO photocatalyst had better sunlight photocatalytic activity than pure ZnO for the decolorization of MB.

3.2.2. Mineralization of MB

COD and TOC removal efficiencies of 40 mg L^{-1} MB solutions by the prepared pure ZnO and Sn-doped ZnO photocatalyst under sunlight irradiation are shown in Fig. 7. It can be seen that COD and TOC removal efficiencies were increasing with the increase

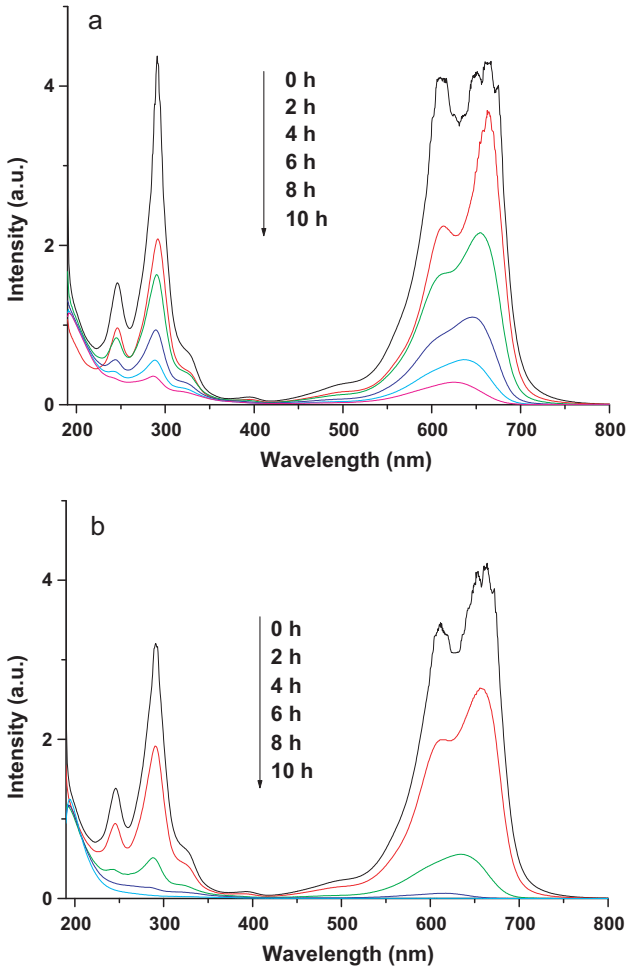

Fig. 6. Adsorption changes of MB aqueous at outdoor temperature (28–36 °C) in the presence of pure ZnO (a) and Sn-doped ZnO (b) under sunlight irradiation.

of reaction time, almost 100% COD and TOC removal efficiencies were achieved within 10 h reaction time for Sn-doped ZnO, while 48% COD removal and 71% TOC removal for the pure ZnO. The results show that MB molecule can be more effectively mineralized by Sn-doped ZnO photocatalyst than by pure ZnO under sunlight irradiation. We proposed that this might have relation to different adsorption characters of pure ZnO and Sn-doped ZnO photocatalyst. There is no significant difference in BET surface areas for pure ZnO and Sn-doped ZnO, therefore, the main reason for the variation in photocatalytic activity for these two samples may be the difference in their pore structures. As shown in Table 1, Sn-doped ZnO has larger pore diameter and pore volume, which may offer more channels for dye molecule. In order to certify our assumption, the comparison removal of MB through physical adsorption by the two photocatalysts was explored. The results showed that about 2.9% COD removal and 2.6% TOC removal for pure ZnO after 30 min adsorption in dark with magnetically stirred, while 4.6% COD removal and 3.6% TOC removal for Sn-doped ZnO. Therefore, a small adsorption ratio of pure ZnO may result in a small decolorization and TOC removal efficiency. But there may be other factors affect the enhancement of photocatalytic activity of Sn-doped ZnO, such as Sn–ZnO heterojunction, high adsorption of dyes and a higher adsorption of light. Additionally, it can be seen that the mineralization rate is slower than the decolorization rate by comparing Figs. 6 and 7. This suggested that the chromophore of MB molecular was more easily destructed for the sunlight photocatalytic degradation of MB by the prepared photocatalyst, and then the degradation intermediates with small molecular were further mineralized to CO_2 and H_2O.

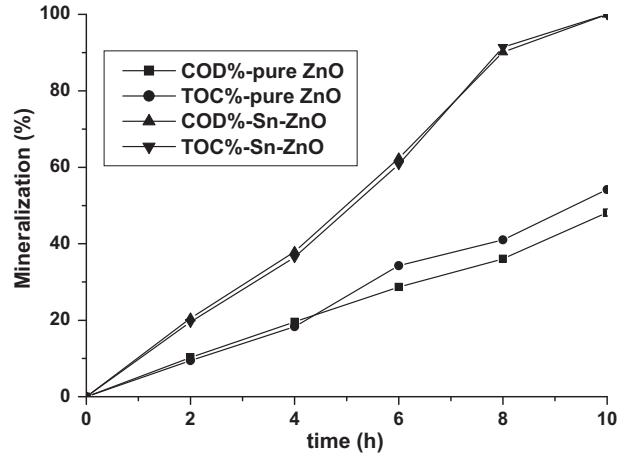

Fig. 7. Mineralization of 300 mL 40 mg L^{-1} MB in the presence of pure ZnO and Sn-doped ZnO photocatalyst under sunlight irradiation.

4. Conclusion

Nano-sized ZnO and Sn-doped ZnO photocatalysts with high photocatalytic activity were successfully synthesized through the decomposition of zinc acetate and glucose by microwave heating. The characterization results showed that the microstructure, morphology and optical properties of ZnO were greatly changed by doping. Sn dopant also greatly increased the photocatalytic activity of ZnO to MB. Compared to pure ZnO, 13% higher decolorization rate, 52% higher COD removal and 29% higher TOC removal efficiency were obtained by the Sn-doped ZnO. The Sn-doped ZnO sample shows higher photocatalytic activity than pure ZnO, which can be attributed to the Sn–ZnO heterojunction, higher adsorption of dyes and light. The Sn-ZnO heterojunction improves the separation of photogenerated electron–hole pairs, thus enhancing the photocatalytic activity. Furthermore, the Sn-doped ZnO sample might more easily excite due to its special optical properties, also leading to higher photocatalytic activity. A more detailed investigation about the effect of doped ions on the photocatalytic activity of ZnO is underway.

Acknowledgements

This work was financial supported by the Basic Scientific and Technological Frontier Project of Henan Province, PR China (Grant No. 102300410098).

References

[1] H. Kyung, J. Lee, W. Choi, Environ. Sci. Technol. 39 (2005) 2376–2382.
[2] I. Yurii, M. Meytal, M. Sheintuch, Ind. Eng. Chem. Res. 37 (1998) 309–326.
[3] A. Criscuoli, J. Zhong, A. Figoli, M.C. Carnevale, R. Huang, E. Drioli, Water Res. 42 (2008) 5031–5037.
[4] N. Daneshvar, M. Rabbani, N. Modirshahla, M.A. Behnajady, J. Photochem. Photobiol. A 168 (2004) 39–45.
[5] J.H. Sun, Y.K. Wang, R.X. Sun, S.Y. Dong, Mater. Chem. Phys. 115 (2009) 303–308.
[6] A.N. Rao, B. Sivasankar, V. Sadasivam, J. Hazard. Mater. 166 (2009) 1357–1361.
[7] J. Wang, Z. Jiang, L.Q. Zhang, P.L. Kang, Y.P. Xie, Y.H. Lv, R. Xu, X.D. Zhang, Ultrason. Sonochem. 16 (2009) 225–231.
[8] M. Muruganandham, J.J. Wu, Appl. Catal. B: Environ. 80 (2008) 32–41.
[9] J.C. Lee, S. Park, H.J. Park, J.H. Lee, H.S. Kim, Y.J. Chung, J. Electroceram. 22 (2009) 110–113.
[10] A.A. Khassin, T.M. Yurieva, V.V. Kaichev, V.I. Bukhtiyarov, A.A. Budneva, E.A. Paukshtis, V.N. Parmon, J. Mol. Catal. A 175 (2001) 189–204.
[11] S.F. Chen, W. Zhao, W. Liu, S.J. Zhang, Appl. Surf. Sci. 255 (2008) 2478–2484.
[12] S. Rehman, R. Ullah, A.M. Butt, N.D. Gohar, J. Hazard. Mater. 170 (2009) 560–569.

[13] L.R. Zheng, Y.H. Zheng, C.Q. Chen, Y.Y. Zhan, X.Y. Lin, Q. Zheng, K.M. Wei, J.F. Zhu, Inorg. Chem. 48 (2009) 1819–1825.
[14] C. Wang, X.M. Wang, B.Q. Xu, J.C. Zhao, B.X. Mai, P.A. Peng, G.Y. Sheng, J.M. Fu, J. Photochem. Photobiol. A 168 (2004) 47–52.
[15] H. Benelmadjat, B. Boudine, O. Halimi, M. Sebais, Opt. Laser Technol. 41 (2009) 630–633.
[16] J. Wang, Y.P. Xie, Z.H. Zhang, J. Li, X. Chen, L.Q. Zhang, R. Xu, X.D. Zhang, Sol. Energy Mater. Sol. C 93 (2009) 355–361.
[17] Z.J. Yang, L.L. Lv, Y.L. Dai, Z.H. Xv, D. Qian, Appl. Surf. Sci. 256 (2010) 2898–2902.
[18] W.D. Yu, X.M. Li, X.D. Gao, F. Wu, J. Phys. Chem. B 109 (2005) 17078–17081.
[19] Y. Zhang, W.F. Zhang, H.W. Zheng, Scripta Mater. 57 (2007) 313–316.
[20] G. Colón, M.C. Hidalgo, J.A. Navío, E.P. Melián, O.G. Díaz, J.M. Doña Rodríguez, Appl. Catal. B: Environ. 83 (2008) 30–38.
[21] S.M. Wang, Z.S. Yang, M.K. Lu, Y.Y. Zhou, G.J. Zhou, Z.F. Qiu, S.F. Wang, H.P. Zhang, A.Y. Zhang, Mater. Lett. 61 (2007) 3005–3008.
[22] I.A. Siddiquey, T. Furusawa, M. Sato, N. Suzuki, Mater. Res. Bull. 43 (2008) 3416–3424.
[23] C.Y. Lee, S.J. Kim, I.S. Hwang, J.H. Lee, Sens. Actuators B Chem. 142 (2009) 236–242.
[24] X.Y. Ye, Y.M. Zhou, Y.Q. Sun, J. Chen, Z.Q. Wang, J. Nanopart. Res. 11 (2009) 1159–1166.
[25] J.G. Yu, X.X. Yu, Environ. Sci. Technol. 42 (2008) 4902–4907.
[26] APHA, Standard Methods for the Examination of Water and Wastewater, 21st edition, 2005, APHA/AWWA/WEF, pp. 5–16 to 5–17, 5220C.
[27] S.Y. Bae, C.W. Na, J.H. Kang, J. Park, J. Phys. Chem. B 109 (2005) 2526–2531.
[28] Q. Xiao, L.L. Ouyang, J. Alloy Compd. 479 (2009) L4–L7.
[29] L.S. Wang, M.W. Xiao, X.J. Huang, Y.D. Wu, J. Hazard. Mater. 161 (2009) 49–54.
[30] D.D. Guo, C.H. Wu, H. Jiang, Q.N. Li, X.M. Wang, B.A. Chen, J. Photochem. Photobiol. B 93 (2008) 119–126.
[31] S.J. Li, Z.C. Ma, J. Zhang, Y.S. Wu, Y.M. Gong, Catal. Today 139 (2008) 109–112.
[32] K.C. Barick, S. Singh, M. Aslam, D. Bahadur, Micropor. Mesopor. Mater. 134 (2010) 195–202.
[33] Z.G. Chen, A. Ni, F. Li, H. Cong, H.M. Cheng, G.Q. Lu, Chem. Phys. Lett. 434 (2007) 301–305.
[34] H.Q. Wang, Z.B. Wu, Y. Liu, Z.Y. Sheng, J. Mol. Catal. A: Chem. 287 (2008) 176–181.
[35] E.M. Seftel, E. Popovici, M. Mertens, E.A. Stefaniak, R.V. Grieken, P. Cool, E.F. Vansant, Appl. Catal. B: Environ. 84 (2008) 699–705.
[36] D. Heger, J. Jirkovsky, P. Klan, J. Phys. Chem. A 109 (2005) 6702–6709.